Journal of Computers Vol. 34 No. 2, April 2023, pp. 233-246
doi: 10.53106/199115992023043402018

A Computer-Aided Intelligent Fault Diagnosis Method for Axial Hydraulic Piston Pump

Yi-Hui Chen*

Tangshan Polytechnic College,
Tangshan City 063000, Hebei Province, China
hy20230202@163.com

Received 1 March 2023; Revised 16 March 2023; Accepted 17 March 2023

Abstract. Axial hydraulic piston pump is widely used in industrial production due to its high pressure resistance and large displacement characteristics, but high pressure and large displacement are also the main causes of piston pump failure. Starting from the fault mechanism of the axial hydraulic piston pump, this paper analyzes and studies the signal characteristics of the fault, and establishes the fault signal acquisition and analysis model. Finally, it discusses the construction of the diagnosis system from both hardware and software, so that the processed typical fault signals can be sent into the intelligent diagnosis system to determine the fault type. Finally, the method in this paper is verified by experiments, which proves the reliability and effectiveness of the diagnosis system.

Keywords: hydraulic piston pump, fault diagnosis, artificial intelligence, time-frequency analysis

1 Introduction

Hydraulic transmission technology is an indispensable part of industrial production process. Axial hydraulic piston pump is the most widely used hydraulic power component in large hydraulic system because of its characteristics of high pressure and large displacement. Once the hydraulic pump breaks down, it will bring economic losses to the enterprise at the light level, and cause machine damage and human death at the heavy level. Axial hydraulic piston pump is a combination of rotary and linear motion. There are many friction pairs and rotary pairs. Therefore, high-pressure, high-speed and reciprocating operation scenarios will accelerate the aging and damage of the piston pump. Typical faults of axial hydraulic piston pump include sliding shoe pair wear, plunger pair wear, loose shoe failure, shoe off failure, center spring fatigue, etc. Aiming at the common plunger pump faults, this paper proposes a new plunger pump fault diagnosis method combined with mature artificial intelligence means to realize the early warning and diagnosis of plunger pump faults and reduce economic losses. The work done in this paper is as follows:

1) Firstly, the fault mechanism of hydraulic pump is analyzed, and the fault signal acquisition and analysis mechanism is established according to the fault phenomenon;

2) Combining time-frequency analysis with neural network, and then using Bayesian optimization algorithm to optimize model parameters, finally achieving the improvement of fault identification accuracy;

3) The overall framework of the diagnosis system is built from both hardware and software dimensions, and the feasibility and efficiency of the method in this paper are verified by experiments.

In order to discuss the method proposed in this paper in detail, the structure of this paper is divided into the following chapters: Chapter 2 mainly studies and analyzes the relevant achievements of relevant scholars at present, and provides research ideas for this method. Chapter 3 mainly discusses the establishment process of typical fault diagnosis model of plunger pump, and Chapter 4 discusses the hardware construction and software flow design in the monitoring and diagnosis system, the fifth chapter mainly demonstrates the feasibility and effectiveness of the algorithm through experiments, the last chapter is the conclusion.

* Corresponding Author

2 Related Work

Relevant scholars have carried out corresponding research on the fault diagnosis of axial hydraulic piston pump and made certain achievements. Azadeh A, explored the aging mechanism of hydraulic pump under high-speed and high-pressure environment, and proposed the artificial intelligence diagnosis method based on data-driven [1]. Maamar Ali Saud ALTobi, contrastively studied the classification of fault states of centrifugal pumps, and used continuous wavelet transform of three different wavelet functions to extract fault features [2]. Based on the excellent classification performance of support vector machine, Janani SR proposed a fault diagnosis model of support vector machine based on artificial fish swarm algorithm, which improved the accuracy of fault classification [3]. Gonalves according to the characteristics of centrifugal pump fault vibration signal, proposed a fault diagnosis method of centrifugal pump combining autoregressive spectrum analysis and hidden Markov model. The algorithm is simple and efficient [4]. Chen Xiangsong, a Chinese scholar, proposed an anomaly detection method of plunger pump based on random convolution kernel by using the pulsation component of the outlet pressure of the plunger pump. Only the pressure pulsation data of the plunger pump under normal conditions can detect the abnormal operation [5]. Ma Haiying, taking the model 25YCY axial piston pump as the test object, made improvements in the method of obtaining vibration signals, and incorporated more convolutions into the monitoring model. Finally, the effectiveness of the method was confirmed in practical production [6]. Xu Changling, proposed a fault diagnosis method of axial piston pump based on deep one-dimensional convolution neural network (D-1DCNN), collected typical vibration signals of piston pump fault, and used them as training data to train the network structure. The final experiment shows that the fault diagnosis rate can reach 100% [7].

3 Establishment of Fault Diagnosis Model for Hydraulic Pump

The structure of axial piston pump mainly includes: valve plate, swash plate, transmission shaft, sliding shoe, plunger, center spring, etc., as shown in Fig. 1, the typical structure of piston pump. Loose shoes, sliding shoes, swashplate wear and spring failure are typical plunger pump failures [8].

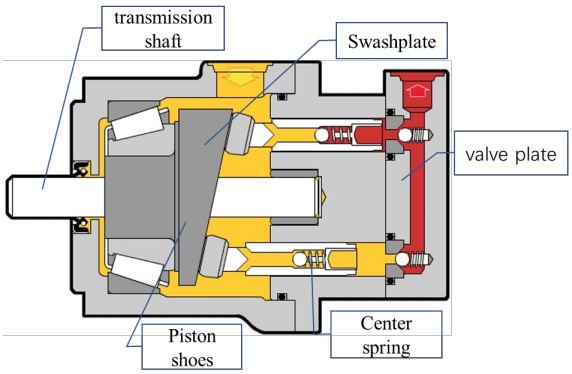

Fig. 1. Plunger pump structure

3.1 Typical Failure Mechanism of Plunger Pump

Due to the machining and assembly errors of the hydraulic pump and the impact in use, the plunger ball head and ball socket will be deformed, resulting in the gap between them becoming larger and causing the loose shoe fault. Loose shoe failure is the main cause of hydraulic shock and high-frequency vibration of the whole hydraulic pump housing. The sliding shoe wear is due to the sliding friction between the sliding shoe and the swashplate, and there is a combination of rotation and revolution. The sliding shoe wear is the main reason for the sliding shoe to fall off and drive failure.

3.2 Time-frequency Analysis Method

Synchronized Wavelet Transforms (SWT) is a method that combines synchronous compression transform with CWT to improve time-frequency resolution by compressing and rearranging the CWT wavelet transform coefficients in the frequency direction [9]. The frequency resolution process of SWT is as follows:

$$W_s(a,b)=\frac{1}{2\pi}\int\frac{1}{\sqrt{a}}\hat{s}(\xi)\psi^*(a\xi)e^{ib\xi}d\xi \tag{1}$$

$W_s(a,b)$ is the wavelet change coefficient, $*$ is the conjugate, $\hat{s}(\xi)$ is the Fourier transform of signal $s(t)$, ξ is the angular frequency, $\widehat{\psi}(\xi)$ is the Fourier transform of $\psi(t)$, and a is the scaling factor. Fourier transform of time-varying signal $s(t)=A\cos(\omega t)$ is:

$$\hat{s}(\xi)=\pi A[\delta(\xi-\omega)+\delta(\xi+\omega)] \tag{2}$$

Therefore, the improved wavelet transform formula is expressed as:

$$W_s(a,b)\quad\frac{A}{2\sqrt{a}}\widehat{\psi}\ (a\xi)e^{ib\xi} \tag{3}$$

If $\widehat{\psi}(\xi)$ tends to zero in the negative frequency domain and ξ is concentrated at $\xi=\omega_0$, then the wavelet coefficient $W_s(a,b)$ is concentrated at the time scale $a=\omega_0/\omega$. The instantaneous frequency $\omega_s(a,b)$ can be estimated by solving the partial derivative of $W_s(a,b)$, which is expressed as follows:

$$\omega_s(a,b)=\begin{cases}\dfrac{-i\partial_b W_s(a,b)}{W_s(a,b)} & W_s(a,b)\neq 0\\ \infty & W_s(a,b)=0\end{cases} \tag{4}$$

The principle of synchronous wavelet transform is to transform $W_s(a,b)$ from the time scale plane to a new time-frequency map. Relying on synchronous compression transform, the (b,a) to $(b,\omega_s(a,b))$ mapping is established. The value of synchronous compression transform $T_s(\omega_t,b)$ is expressed as:

$$T_s(\omega_c,b)=(\Delta\omega)^{-1}\sum_{a_k:|\omega(a_k,b)-\omega_c|\Delta\omega/2}W_s(a_k,b)a_k^{-\frac{3}{2}}(\Delta a)_k \tag{5}$$

The inverse transform of synchronous compression wavelet is:

$$s(t)=\mathrm{Re}\left[C_\psi^{-1}\sum_c T_s(\omega_c,b)(\Delta\omega)\right] \tag{6}$$

$$C_\psi^{-1}=\int_0^{+\infty}\widehat{\psi}^*(\xi)\frac{d\xi}{\xi} \tag{7}$$

Where, a_k is the discrete scale, Re is the real part, and $a_k-a_{k-1}=(\Delta a)_k$ is the center frequency:

$$\omega_t \in \left[\omega_c - \frac{1}{2}\Delta\omega, \omega_c + \frac{1}{2}\Delta\omega\right] \tag{8}$$

3.3 Improved Convolution Neural Network Model

This paper takes the vibration time-frequency information of the axial hydraulic piston pump body as the input feature, uses the improved ResNeSt classic convolution network structure as the backbone network, then fuses the time-frequency analysis with the improved network model, and finally uses the Bayesian adaptive optimization algorithm to set the model parameters to complete the creation of the model.

In the ResNeSt structure, the jump connection structure is added to make the network transmission more in-depth. At the same time, the coordinate attention mechanism is added to the feature extraction unit to carry out the weighted fusion of features. Finally, the low-level activation function is canceled. After the above improvement, the recognition accuracy of the network can be improved. The improved algorithm structure is shown in Fig. 2.

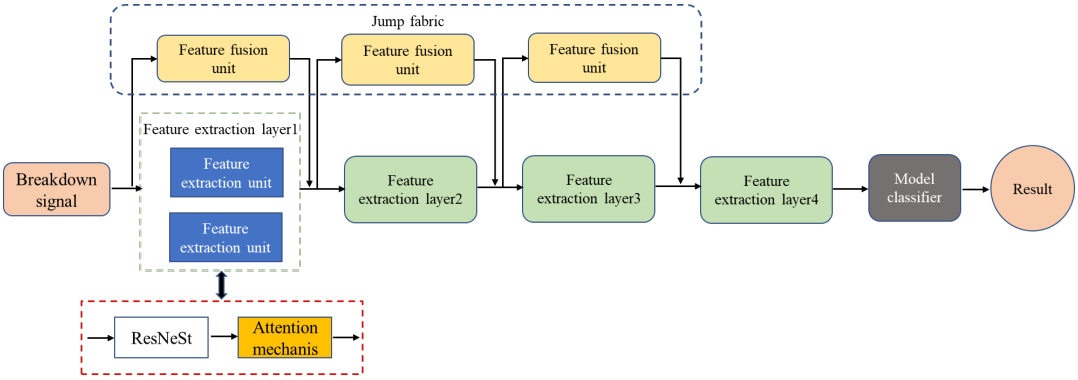

Fig. 2. Improved algorithm structure

1) Design of jump connection structure

In the feature extraction structure of the ResNeSt network model, image features are gradually introduced from the shallow layer of the network to the deep layer of the network through jump connection, and are fused with the deep image features, so as to better solve the problem of information loss in the transmission process of local detail features from the shallow layer to the deep layer of the network. The feature fusion unit adjusts the dimension, width and height of the input feature map of feature extraction layer i_1, as shown in Fig. 3.

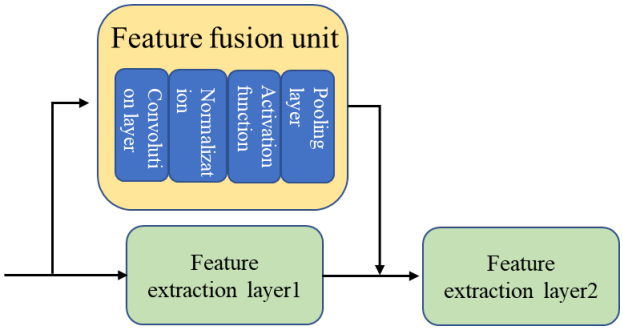

Fig. 3. Jump fabric

Assuming that the input feature information I_1 of feature extraction layer 1 is $C_1H_1W_1$ and the output feature information is $C_2H_2W_2$, the input feature information I_2 of feature extraction layer 2 is expressed as:

$$I_2 = \sigma(T(C_1H_1W_1)) + C_2H_2W_2 \tag{9}$$

Where, σ represents the maximum pooling operation with a step size of 2, T represents the convolution operation with a convolution kernel size of 1, C_1 and C_2 represent the number of channels of input and output features, H_1 and W_1 represent the height and width of input features in feature extraction layer 1, and H_2 and W_2 represent the height and width of output features in feature extraction layer 1.

2) Introduction of coordinate attention mechanism module

The attention mechanism module can help screen out features that are more beneficial to network training [10]. The schematic diagram of coordinate attention mechanism is shown in Fig. 4.

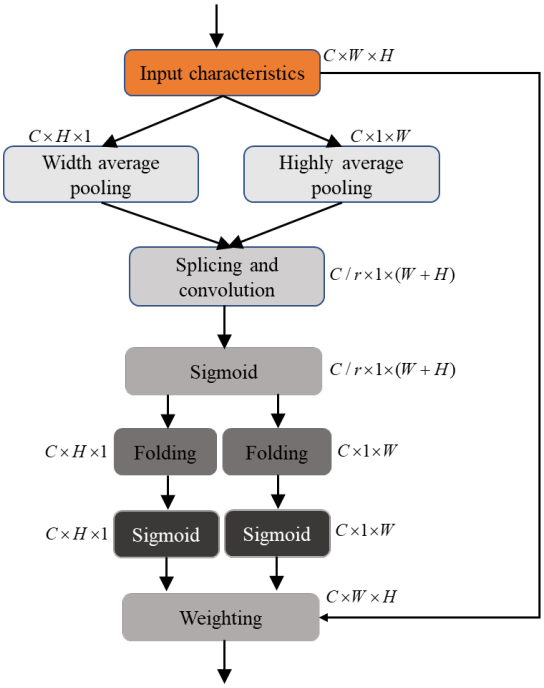

Fig. 4. Schematic diagram of attention mechanism

Step 1: The coordinate attention module uses pooled cores $(H,1)$ and $(1,W)$ to integrate the input feature map along the width and height directions, and finally obtain the feature map in the width and height directions. The output of channel c with width w can be expressed as:

$$z_c^w(w) = \frac{1}{H} \sum_{0 \le j \le H} x_c(j,w) \tag{10}$$

The output of channel c of height h can be expressed as:

$$z_c^h(h) = \frac{1}{W} \sum_{0 \le i \le W} x_c(h,i) \tag{11}$$

Step 2: splice the feature maps in the width and height directions of the global receptive field and send them to the convolution module with the convolution core of 1×1, reduce the dimension to the original C/r, and finally obtain the $1\times(W+H)\times C/r$ feature map through the *Sigmoid* activation function. The output is expressed as follows:

$$f=\delta(F_1([z^h,z^w])) \tag{12}$$

Where δ is the activation function of *Sigmoid*, F_1 is the convolution transformation function, $[\cdot,\cdot]$ is the splicing, $f\in R^{C/r\times(H+W)}$ is the intermediate feature containing the width kernel height information, and r is the reduction factor.

Step 3: Divide f into two feature maps f^w and f^h, and obtain the attention weight g^w in the width direction and the attention weight g^h in the height direction of the feature map after the activation function processing. The formula is expressed as follows:

$$g^w=\delta(F_w(f^w)) \tag{13}$$

$$g^h=\delta(F_h(f^h)) \tag{14}$$

F_w and F_h represent the convolution transformation of 1×1.

Step 4: Through multiplication and weighting calculation on the original feature map, the final feature map with attention weight in the width and height directions will be obtained, and the result can be expressed as:

$$y_c(i,j)=x_c(i,j)\times g_c^h(i)\times g_c^w(j) \tag{15}$$

3) Optimization of model classifier structure

There are only 127 types of defects in axial hydraulic piston pump identified in this paper, which is far lower than the channel dimension of the full connection layer, resulting in redundant feature information mixing into the channel and reducing the accuracy of feature recognition. Therefore, the activation function and two layers of the last layer of the network structure are removed from the model classifier, and the number of convolution layer channels are re-matched according to the plunger defect classification. The structure schematic diagram of the final classifier is shown in Fig. 5:

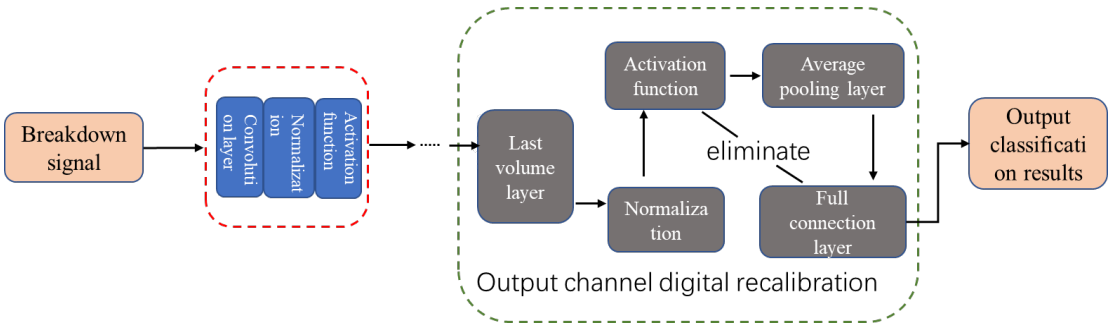

Fig. 5. Classifier structure schematic diagram

ReLU activation function is used in the model classifier to increase the nonlinearity of the neural network model, overcome the problem of model gradient disappearance and improve the speed of data training.

$$\mathrm{Re}\,LU(x)=\begin{cases}x & x\geq 0\\ 0 & x<0\end{cases} \tag{16}$$

When the input is not greater than zero, the activation function is not activated, and the full connection layer plays a role in transforming the features extracted from the previous layer in improving the network structure, thus reducing the dimension. The depth feature is obtained through the above average pooled layer fusion, and the classification results are finally output, thus completing the optimization of the model classifier structure.

3.4 Improved Convolution Neural Network Model

The fusion of time-frequency analysis and convolution network is carried out from the following aspects:

1) The fusion object is vibration, sound, pressure and other multi-source signals in the axial hydraulic piston pump body, mainly vibration signals, which is the basis of nondestructive monitoring;

2) Through time-frequency analysis, the one-dimensional vibration signal in the piston pump fault is transformed into a two-dimensional time-frequency characteristic image, and then sent to the neural network for feature extraction.

3) The fusion method improves the recognition accuracy and recognition ability. The transformed vibration signal of the axial hydraulic piston pump is used as the input of the convolution network [11]. After the multi-layer convolution network feature extraction, the hidden information of the feature map can be automatically learned, and the abstract feature extraction of the original signal can be realized.

4) Bayesian algorithm is used to automatically search for the optimal parameters and adaptively adjust the training level of the algorithm model to complete the creation of the model [12]. Bayesian algorithm is a combination of Gaussian function and acquisition function. When selecting the covariance function and mean function of Gaussian formula, the data distribution is assumed to be Gaussian distribution, and then the mean function and covariance function are used. The expression is as follows:

$$f(n_{1:t})\sim Normal[\chi(n_{1:t}),C^{\theta}(n_{1:t},n_{:t})_{ij}] \tag{17}$$

Where, $\chi(n_{1:t})=\chi(n_i)$ is the mean vector and $C^{\theta}(n_{1:t},n_{1:t})_{ij}=C^{\theta}(n_i,n_j)$ is the covariance matrix. The Matérn5/ 2 covariance is used as the kernel function, and the mean function is zero mean. The covariance calculation formula can be expressed as:

$$C^{\theta}_{M5/2}(n_i,n_j)=\exp(-\sqrt{5}r)(1+\sqrt{5}r+\frac{5}{3}r^2) \tag{18}$$

$$r=(n_i-n_j)^T\,diag(\theta^2)^{-1}(n_i-n_j) \tag{19}$$

Where, $diag$ represents diagonal matrix. Then use the expectation promotion strategy to evaluate the objective function. The mathematical expression is:

$$\eta_{EI}(X;\theta,D)=E[\max(0,f(X)-f(X^*))] \tag{20}$$

The Gaussian process is further expressed as:

$$\eta_{EI}(X;\theta,D)=\rho_t(X;\theta,D)[x\Phi(x)+\phi(x)] \tag{21}$$

$$x=\frac{\mu_t(X;\theta,D)-f(X^*)}{\rho(X;\theta,D)} \tag{22}$$

$f(X^*)$ is the current best value, $f(X)$ is the best target, Φ is the cumulative distribution function, ϕ is the composite standard normal distribution probability density function, μ_t is the expected value, $\mu(\theta^*)$ is the best expected value in the average result, and the expected increase can be expressed as:

$$\begin{cases} \eta_{EI}(X;\theta,D) = \rho_t(X;\theta,D)[\lambda\Phi(\lambda)+\phi(\lambda)] \\ \lambda = \dfrac{\mu_t(X;\theta,D)-\mu(\theta^*)}{\rho(X;\theta,D)} \end{cases} \tag{23}$$

Through the above process, the fusion and Bayesian optimization are completed.

4 Design of Intelligent Monitoring System

This section completes the simulation experiment and status data collection of typical faults of plunger pump, and then converts the one-dimensional signal to identify using the network structure in the previous section to complete the fault diagnosis.

4.1 Hardware Composition of Experimental System

The experiment uses the hydrodynamic transmission and control experimental platform of an enterprise in Hebei Province as the experimental platform. The photos of the experimental platform are shown in Fig. 6. The models and parameters of the main hardware of the experimental platform are shown in Table 1.

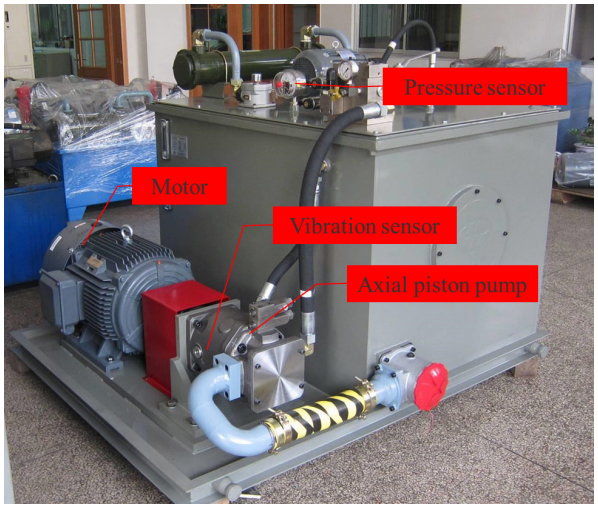

Fig. 6. Hydraulic test system

Table 1. Hardware model and parameters of hydraulic pump test platform

Name	Model	Main parameter
Power motor	YE2-7134	1450r/min
Axial hydraulic plunger pump	V50A4R10X	Nominal pressure 32.3MPa, displacement 11ml/r, plunger quantity 7.
Hydraulic pump station	/	0-28MPa

Vibration acceleration sensor	YD72D	Charge sensitivity 0.35Pc/ms^{-2}, frequency range 1-18kHz, amplitude range1000ms^{-2}
Charge amplifier	DHF-10	Output voltage ±10V, gain 1-100Mv/pC, frequency response range 0.1-100kHz, 2 channels, which can be used for charge amplification and conversion of 3-way acceleration sensor
Regulated power supply	WYT-302	Output voltage 0-30V, output current 0-2A
Data acquisition card	NI USB-6221	16-channel analog input, 16-bit precision, sampling rate255kS/s, update rate833kS/s, 24-channel I/O port
IPC	Inter(R) Core(TM)2 CPU	1.86GHz, 2GB memory, 200G high-speed hard disk, 4 USB bus interfaces

4.2 Fault Element Setting

According to the above contents and engineering practice, the typical faults of axial hydraulic piston pump include loose shoe fault, sliding shoe wear, swashplate wear, center spring failure, etc. This paper mainly aims at the identification and diagnosis of the loose shoe and wear fault of the sliding shoe, sets the different loose shoe degrees between the sliding shoe and the plunger head of the experimental platform, and takes the grinding of the sliding shoe bottom surface to different degrees as the fault source, as shown in Fig. 7.

Fig. 7. Schematic diagram of different faults

4.3 Flow Chart of Intelligent Diagnosis System

The whole fault diagnosis system includes four functional modules: data acquisition module, data preprocessing module, model training and optimization module, and model recognition and diagnosis module. In the data acquisition stage, the vibration signal sensor and sound sensor installed on the axial hydraulic pump body collect the one-dimensional time domain signal. The data preprocessing module converts one-dimensional time-domain signal into two-dimensional time-frequency spectrum through time-frequency analysis, and divides a certain proportion as model training set and test set. The model training and optimization module, as described in Chapter 3, improves the neural network structure, and then uses Bayesian algorithm to search the optimal parameters. Finally, after the model recognition diagnosis module is trained with the atlas, the diagnosis model can be applied to the fault diagnosis of the measured state data. After the state sample is input, the corresponding state prediction tag value can be obtained through the automatic learning of the diagnosis model, and the final fault classification recognition result can be obtained directly. The system flow chart is shown in Fig. 8.

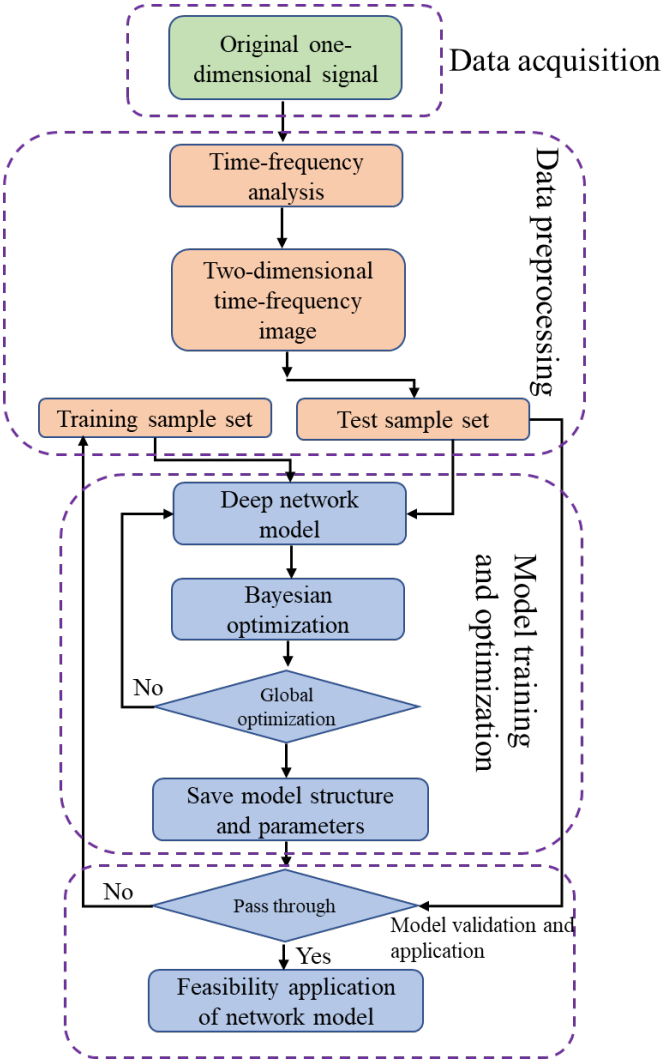

Fig. 8. System flow chart

5 Experimental Results and Analysis

The experimental equipment and framework are designed as a deep learning framework, Python 1.5.1, which is programmed independently in Python language. The calculation configurations are: Dell Precision T5820 workstation, Intel Xeon processor W-2235 (6 C, 3.8 GHz), NVIDIA graphics card RTX4000 (8 GB video memory), memory (32 GB, 2666 MT/s), hard disk (2 TB mechanical+512 G solid state).

5.1 Vibration Signal Acquisition

Taking the parameter setting of working pressure 20 MPa and sampling frequency 12 kHz as an example, the collected vibration time domain signals of axial piston pump under different conditions are shown in Fig. 9. In the experiment, the time required for each rotation of the hydraulic pump is about 0.05 s.

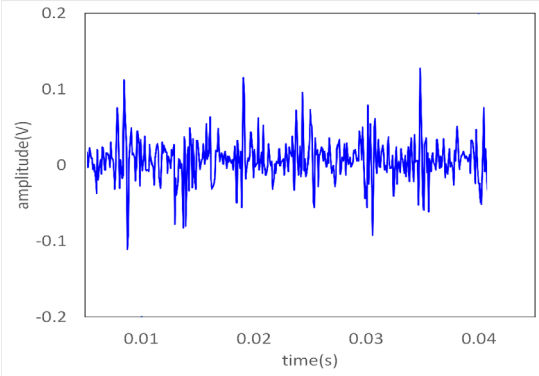

(a) Normal state

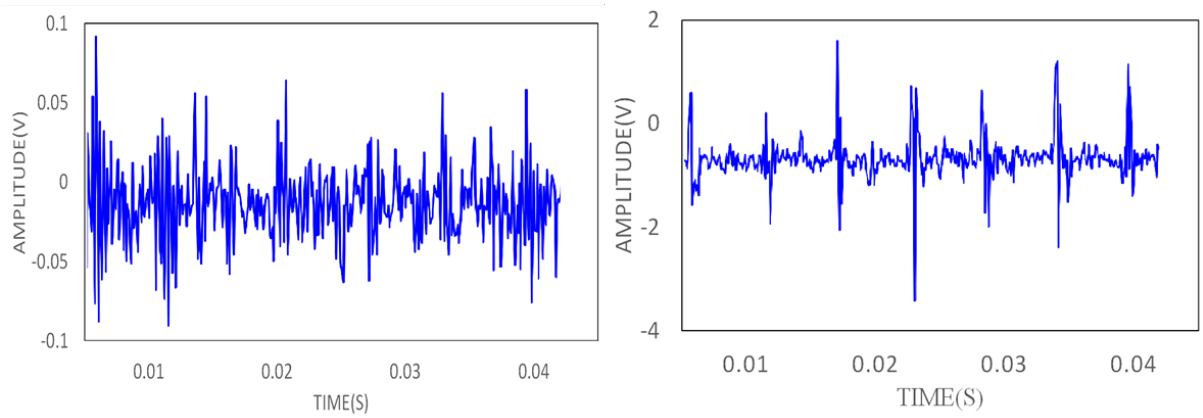

(b) Shoe wear (c) Loose shoe fault

Fig. 9. Hydraulic pump vibration signal

5.2 Time-frequency Transformation of Signal and Model Training

SWT parameter setting: the synchronous compression wavelet transform function is used, the bandwidth and center frequency are set to 3, and the scale sequence length is 256. Taking working pressure 15MPa as an example, after SWT transformation, the two-dimensional image of hydraulic pump vibration signal is shown in Fig. 10.

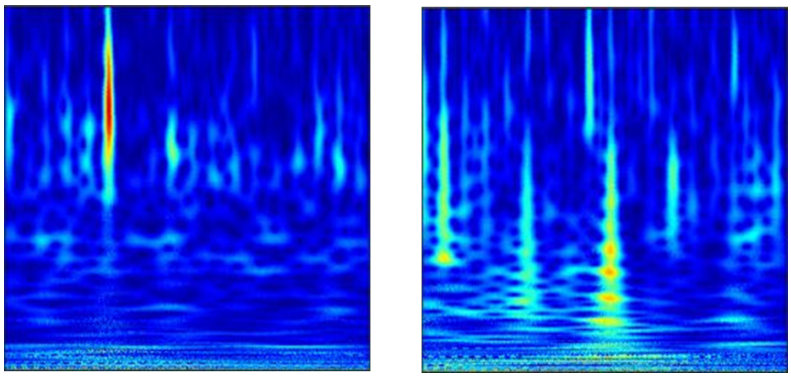

(a) Fault two-dimensional image (b) Shoe wear

Fig. 10. Fault two-dimensional image

After converting into two-dimensional time-frequency domain graphics, model training sets and test sets are constructed. In this paper, the training sets and test sets of the fault sample library are set according to the 7:3 ratio. A total of 2400 samples are collected from the vibration signal samples of loose shoe failure and sliding shoe wear under different outlet pressures and converted into time-frequency spectra. The sample division and label identification are shown in Table 2.

Table 2. Sample division and identification

Fault name	Number of training samples	Number of test samples	Sample label
Loose shoe fault	840	360	0
Shoe wear	840	360	1
Summation	1680	720	

5.3 Analysis of Diagnosis Results

Set the number of iterations of the model to 100. The model iteration process is shown in Fig. 11.

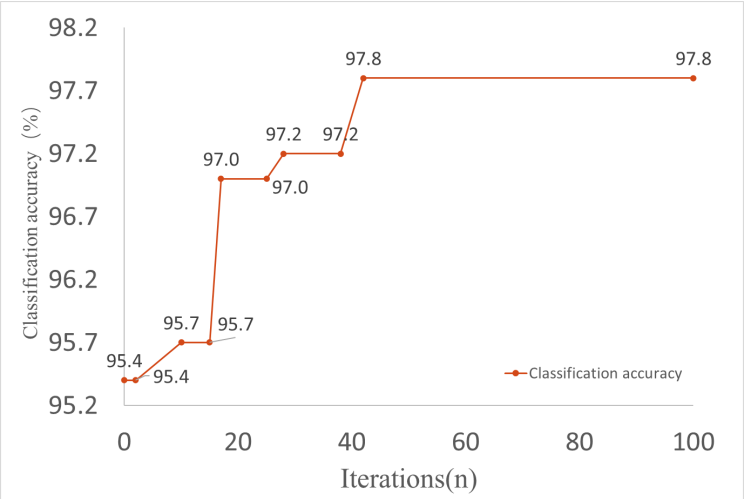

Fig. 11. Algorithm optimization iteration process

It can be seen from the above figure that when the number of iterations is greater than 40, the convergence has begun. After 8 times of repeated training for the model, the less the training loss, the better the convergence of the model. From the training accuracy curve, it can be seen that the gap between the training samples and the test samples is small, indicating that the recognition accuracy of the model is improved and the stability is enhanced. In order to prove the advantages of the improved model and test system compared with the original ResNeSt model, eight independent experiments were carried out, and the experimental results are shown in Fig. 12.

It can be seen from the figure that compared with the traditional ResNeSt model, the average classification accuracy of the improved ResNeSt model for the two categories of axial piston pump is 3.1% higher, the average classification accuracy of the improved ResNeSt model is 97.65%, and the average classification accuracy of the traditional ResNeSt model is 94.55%

	1	2	3	4	5	6	7	8
After improvement	97.3	98.4	97.9	97.3	97.4	97.2	98.5	97.2
Before improvement	96.2	94.9	93.4	94.2	92.6	94.6	96.8	93.7

Fig. 12. Comparison before and after algorithm improvement

6 Conclusion

In this paper, the one-dimensional vibration signal of the plunger pump is collected after the typical fault occurs, and the wavelet time-frequency analysis method is used to convert the one-dimensional signal into two-dimensional image, and then the converted image is sent to the improved network structure model for recognition. After experimental analysis and comparison, the algorithm proposed in this paper can improve the recognition accuracy by 3 percentage points. Next, we will further analyze and study other typical fault identification of plunger pump to achieve more comprehensive fault diagnosis, and improve the accuracy of identification by nearly 100%.

References

[1] A. Azadeh, M. Saberi, A. Kazem, V. Ebrahimipour, A. Nourmohammadzadeh, Z. Saberi, A flexible algorithm for fault diagnosis in a centrifugal pump with corrupted data and noise based on ANN and support vector machine with hyper-parameters optimization, Applied Soft Computing 13(3)(2013) 1478-1485.

[2] M.A. Saud ALTobi, G. Bevan, P. Wallace, D. Harrision, K.P. Ramachandran, Fault diagnosis of a centrifugal pump using MLP-GABP and SVM with CWT, Engineering Science and Technology, an International Journal 22(3)(2019) 854-861.

[3] J.S. Rapur, R. Tiwari, Experimental fault diagnosis for known and unseen operating conditions of centrifugal pumps using MSVM and WPT based analyses, Measurement 147(2019) 106809.

[4] J.P.S. Goncalves, F. Fruett, J.G.D. Filho, M. Giesbrecht, Faults detection and classification in a centrifugal pump from vibration data using markov parameters, Mechanical Systems and Signal Processing 158(2021) 107694.

[5] X.-S, Chen, J.-F. Tao, C.-L. Liu, Anomaly Detection Method of Axial Pump Based on Random Convolution Kernel and Isolated Forest, Chinese Hydraulics & Pneumatics 47(2)(2023) 26-33.

[6] H.-Y. Ma, P. Zhang, Z.-J. Guo, Optimization and verification of fault diagnosis network for 25YCY piston pump based on 1DCNN, Chinese Journal of Construction Machinery 20(3)(2022) 269-272.

[7] C.-L. Xu, J.-H. Huang, Y. Lan, B. Wu, C.-G. Niu, X.-B. Ma, B. Li, Fault diagnosis of axial piston pump based on D-1DCNN, Journal of Mechanical and Electrical Engineering 38(11)(2021) 1494-1500.

[8] L.-L. Sun, Investigation on Common Faults and Troubleshooting of Hydraulic Pump, Modern Manufacturing Technology and Equipment 57(9)(2021) 159-160.

[9] X.-Q. Wu, Z.-Y. Zou, W. Yan, H.-L. Zhou, X.-F. Liu, PT secondary interference of GIS based on synchronous compression wavelet transform, Electric Power Engineering Technology 40(6)(2021) 134-140.

[10] W. Wang, X.-G. Wan, A small target detection method combining attention mechanism and feature fusion, Journal of

Xi'an Polytechnic University 36(6)(2022) 115-123.
[11] M. Zhou, J.-H. Chang, S.-C. Chen, Y.-Y. Meng, T.-F. Dai, Aerosol Type Recognition Model Based on Naive Bayesian Classifier, Acta Optica Sinica 42(18)(2022) 49-57.
[12] H.-X. Wang, C.-J. Zhang, Y. Liu, B. Guo, Research on Denoising Algorithm of Wavelet Eeg Based on Bayesian Estimation, Journal of Changchun University of Science and Technology (Natural Science Edition) 44(2)(2021) 105-111.